Polybenzimidazole-Based Block Copolymers: From Monomers to Membrane Electrode Assemblies for High Temperature Polymer Electrolyte Membrane Fuel Cells

Frank Schönberger,[1,2] Guoqing Qian,[2] Brian C. Benicewicz[2]

[1]Plastics Division, Fraunhofer Institute for Structural Durability and System Reliability LBF, Schlossgartenstraße 6, Darmstadt 64289, Germany
[2]Department of Chemistry and Biochemistry, University of South Carolina, 541 Main Street, Horizon I Bldg, Columbia, South Carolina 29208
Correspondence to: F. Schönberger (E-mail: frank.schoenberger@lbf.fraunhofer.de)

Received 19 October 2016; accepted 21 January 2017; published online 23 March 2017
DOI: 10.1002/pola.28530

ABSTRACT: In this study, PBI-based block copolymers were developed and their performance as membranes in high temperature polymer electrolyte membrane fuel cells was evaluated. This type of block copolymer consists of "phosphophilic" PBI and "phosphophobic" non-PBI segments. The final properties of such block copolymers strongly depended on the length of the individual blocks and their chemical structures. In a systematic approach, a series of various block copolymers was synthesized and characterized both in terms of *ex situ* properties (e.g., proton conductivity, phosphoric acid uptake, swelling behavior) and *in situ* fuel cell tests. A very poor membrane-electrode interface limited the performance of the membrane electrode assemblies, but was remarkably improved in power output, stability, and long-term durability by treating the electrode interface with a fluorinated PBI derivative. © 2017 Wiley Periodicals, Inc. J. Polym. Sci., Part A: Polym. Chem. **2017**, *55*, 1831–1843

KEYWORDS: block copolymers; high temperature polymer electrolyte fuel cell; membranes; membrane electrode assembly; poly(arylene ether)s; polybenzimidazole; renewable resources; telechelics

INTRODUCTION Phosphoric acid doped polybenzimidazoles (PBIs) are widely used as membrane materials in fuel cell applications at temperatures up to 200 °C and low relative humidities.[1–4] Many polymers of the PBI family have been intensively studied for use in high-temperature polymer electrolyte membrane fuel cells (PEMFCs), among them *meta*- and *para*-PBI,[5] AB-PBI,[6] partially fluorinated PBIs,[7] hydroxylated PBIs,[8] sulfonated PBIs and their blends[9] as well as PBIs containing more than four nitrogen atoms per repeating unit.[10] There are different approaches to tailor the membrane properties to achieve sufficiently high performance and life times, including crosslinking of PBI[11–15] and incorporating inorganic fillers into the membrane.[16,17] Surprisingly, there are only few examples on the preparation and characterization of block copolymers for high-temperature polymer electrolyte membrane fuel cells (HT-PEMFCs) while this concept is commonly used in the field of low-temperature polymer electrolyte membrane fuel cells (LT-PEMFCs).[18–20] McGrath et al. published a concept to structure multiblock copolymers by coupling *ortho*-diamino terminated PBI telechelics with carboxylic acid end-capped poly(arylene ether sulfone) telechelics (PAES) in *N*-methyl-2-pyrrolidinone (NMP).[21] Subsequent doping in PA forms proton-conducting paths in the *meta*-PBI segment of the structure while the PAES segments should be unaffected (providing that no long-term degradation takes places, e.g., by acid-induced ether cleavages)[22] and maintain dimensional and mechanical stability. However, the reported proton conductivities in the range of 0.032 to 0.042 S/cm (at liquid uptake values of about 180 to 200%) appear rather low for the intended use in fuel cells. This might be due to the fact that the block length ratio between PBI and non-PBI segments was kept the same (1: 1) while the length for both blocks was varied at 5, 10, and 15 kDa. Unfortunately, there are no fuel cell data reported for such block copolymers in the literature making it difficult to evaluate these type of block copolymers for real fuel cell applications.[21] Another group published the preparation of crosslinked membranes based on sulfonated poly(arylene ether ketone) and polybenzimidazole oligomers.[23] However, no *in situ* fuel cell data was reported for these types of membranes.

In the current work, we planned to synthesize and characterize (asymmetric) block copolymers with increased block

Additional Supporting Information may be found in the online version of this article.

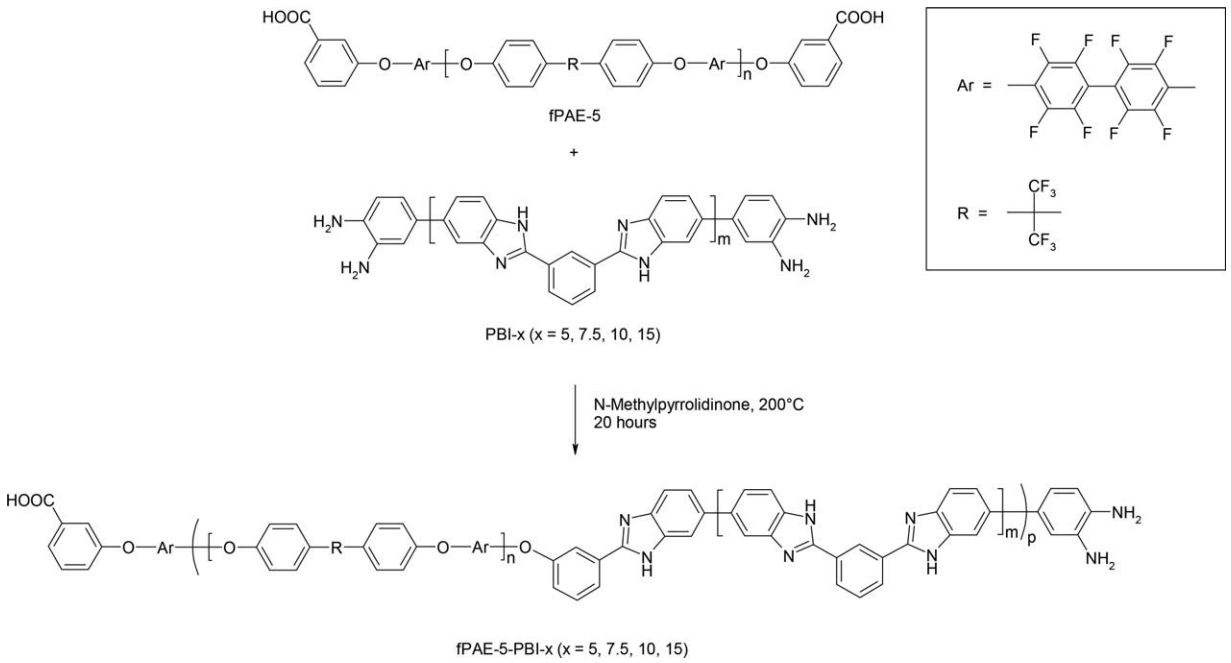

FIGURE 1 Polycondensation reaction between fluorinated poly(arylene ether) and polybenzimidazole telechelics.

length of the PBI segments compared to the length of the non-PBI block (and thereby, enhancing the proton conductivity of the membrane). The block length of the non-PBI segment was kept at 5 kDa while the segment block length of PBI was varied from 5 to 15 kDa (Fig. 1). To expand the diversity of chemical structures, higher "phosphophobic" non-PBI segments were incorporated than the previously used block copolymers with poly(arylene ether sulfone) segments. Unlike poly(arylene ether sulfone), partially fluorinated poly(arylene ether) segments inhibit formation of hydrogen bonds to H_3PO_4 molecules and might help to increase repulsive interaction between the incompatible blocks.[24–26]

Additional aims of the current work were to synthesize and characterize block copolymers with different chemical structures in the non-PBI block (while the block length ratio was kept constant, cf. Fig. 2) to extend the structure–property relationships available concerning the chemical structure for the non-PBI block. Since the properties and in particular the polarities of the various chemical structures differ, one would expect to observe an influence on the membrane properties of the block copolymers. Finally, fuel cell characterization of the membranes is reported on the block copolymer membranes, providing important information that is noticeably missing in the literature on these materials.

EXPERIMENTAL

Materials

3,3′,4,4′-Tetraaminobiphenyl (TAB, polymerization grade, 97.5%) was obtained from BASF Fuel Cells and isophthalic acid from Amoco Chemical Company. Polyphosphoric acid was purchased from Innophos. The chemicals for synthesizing the telechelic macromonomers were supplied from Aldrich (decafluorobiphenyl (99%), bis(4-fluorophenyl)-phosphine oxide (97%)), TCI America (2,2-bis(4-hydroxyphenyl)hexafluoropropane (98%)), Alfa Aesar (4,4′-dichlorodiphenylsulfone (98%), 4,4′-biphenol (99%)), and Acros Chemicals (3-hydroxybenzoic acid (99%)). Bis(4-hydroxyphenyl)phenyl phosphine oxide was prepared via a Grignard reaction from 4-bromophenol (97%), dihydropyrane (99%), and dichlorophenyl phosphine oxide (98%) (all purchased from Acros) and magnesium (Fisher) according to the literature.[27] The monomers were used without further purification. Potassium carbonate (99.8%) from Mallinckrodt was ground and dried at 140 °C in vacuo for 16 h before use. Anhydrous solvents were obtained from EMD Chemicals (*N,N*-dimethylacetamide, DMAc) and from Burdick and Jackson (*N*-methyl-2-pyrrolidinone, NMP).

Synthesis of *Meta*-Polybenzimidazole Telechelic Macromonomers

Meta-PBI telechelic macromonomers with 5, 7.5, 10, and 15 kDa (PBI-5, PBI-7.5, PBI-10, PBI-15) were produced by molecular-weight controlled step-growth polycondensation between 3,3′,4,4′-tetraaminobiphenyl (TAB) and isophthalic acid in polyphosphoric acid similar to the literature.[21] Carother's equation was used to calculate the stoichiometric imbalance of monomers.[28,29] Unlike previous literature, not only was the polycondensation process conducted in a nitrogen atmosphere, but also the entire work-up procedure. The product was stored in nitrogen atmosphere (glove box) until use. Telechelic macromonomers that were worked-up under atmospheric conditions were not completely soluble in NMP and formed significant amounts of microgel particles. Such microgel particles probably resulted from auto-oxidation of diamino end groups via free radical intermediates and their

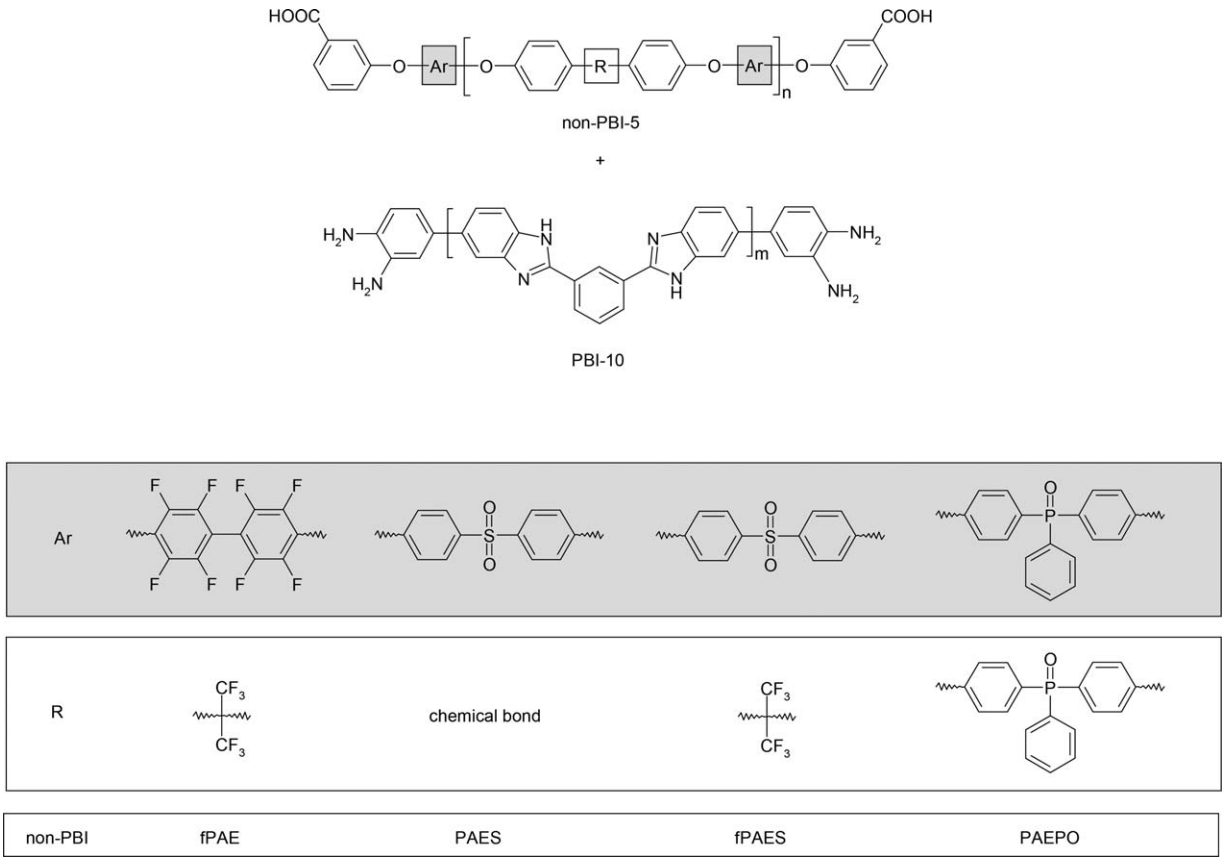

FIGURE 2 Overview of chemical structures varied in the non-PBI segments.

subsequent partial polymerization, similar to the TAB monomer itself.[30,31]

A typical procedure for the synthesis of a telechelic m-PBI macromonomer (5 kDa, PBI-5) is as follows: 5.9040 g (35.5387 mmol) of isophthalic acid and 8.0994 (37.80 mmol) of TAB were mixed with 139.37 g polyphosphoric acid (PPA) in a three-neck 250-mL flask equipped with a nitrogen inlet/outlet and a mechanical stirrer. The mixture was heated stepwise to 200 °C and kept for 17 h at this temperature. The resulting dark brown solution was coagulated in deionized water and stirred for 24 h in a nitrogen atmosphere. Then, the macromonomer was filtered and neutralized with NH_4OH solution while protecting with nitrogen atmosphere. The macromonomer was finally washed with deionized water in nitrogen atmosphere and dried at 130 °C in vacuo for 24 h. It was then immediately transferred into the glove box.

Synthesis of Carboxylic Acid End-Capped Poly(Arylene Ether) Macromonomers

The series of carboxylic acid end-capped telechelic macromonomers with 5 kDa and various chemical structures was synthesized from the corresponding monomers: fluorinated poly(arylene ether) macromonomers (fPAE-5) from decafluorobiphenyl, 2,2-bis(4-hydroxyphenyl)hexafluoropropane, and 3-hydrobenzoic acid; poly(arylene ether sulfone) macromonomers (PAES-5) from 4,4′-dichlorodiphenylsulfone, 4,4′-biphenol, and 3-hydrobenzoic acid; fluorinated poly(arylene ether sulfone) macromonomers (fPAES-5) from 4,4′-dichlorodiphenylsulfone, 2,2-bis(4-hydroxyphenyl)hexafluoropropane, and 3-hydrobenzoic acid; poly(arylene ether phosphine oxide) macromonomers (PAEPO-5) from bis(4-hydroxyphenyl)phenyl phosphine oxide, bis(4-fluorophenyl)phenyl phosphine oxide, and 3-hydrobenzoic acid. None of the poly(arylene ether) homopolymers showed any swelling behavior or weight uptake when placed in phosphoric acid.

A typical synthesis procedure is given for fPAE-5 macromonomer as follows: 7.5343 g (22.41 mmol) of 2,2-bis(4-hydroxyphenyl)hexafluoropropane, 8.6334 g (25.84 mmol) of decafluorobiphenyl, 0.9480 g (6.86 mmol) of 3-hydroxybenzoic acid, and 10 g (72.35 mmol) of potassium carbonate were added to a three-neck 250-mL flask equipped with a condenser, a nitrogen inlet/outlet, and a mechanical stirrer. After addition of anhydrous DMAc (142 mL) the reaction temperature was slowly increased from room temperature to 90 °C and the mixture was stirred for 24 h. After filtering, the resulting viscous solution was coagulated in brine. The telechelic benzoic acid functionality of the telechelic macromonomer was recovered from its potassium salt form by stirring in 0.1 M H_2SO_4 for 24 h. Finally, the macromonomer was isolated by filtration, dried at 110 °C *in vacuo* for 24 h, and immediately transferred into the glove box.

Synthesis of Poly(Arylene Ether)-*Block-Meta*-Polybenzimidazoles

The series of block copolymers was synthesized by coupling *ortho*-diamino terminated m-PBI telechelic macromonomers and carboxylic acid end-capped poly(arylene ether) telechelic macromonomers in anhydrous *N*-methyl pyrrolidinone (NMP) as a solvent at 200 °C under constant nitrogen flow. Initial macromonomer concentrations were between 5 and 7 wt % depending on the block length ratio. Reaction times and stirring rates had to be adapted individually for each combination. In the following, the coupling reaction between the fPAE-5 and PBI-5 is given as an example: 4.000 g (0.5 mmol) of fPAE-5, 4.1712 g (0.5 mmol) of PBI-5, and 159 mL of anhydrous NMP were added to a three-neck 250-mL flask equipped with a mechanical stirrer, and a nitrogen inlet/outlet. The reaction mixture was heated at 200 °C for 14 h (with a stirring rate of 130 rpm) and for another 7 h (with a stirring rate of 70 rpm). The product was precipitated in water and washed with water several times. Finally, it was dried at 150 °C *in vacuo* for 16 h.

Inherent Viscosity Measurements and NMR Spectroscopy

Inherent viscosity (IV) measurements were taken in a Cannon Ubbelohde viscometer (size 100) in a 30 °C water bath. The concentration of macromonomer or block copolymer was 0.2 g/L in NMP/LiCl (1 wt % LiCl). All samples were passed through a 0.25 μm PTFE syringe filter before injecting into the viscometer. The inherent viscosity was then calculated from the following equation.

$$\mathrm{IV} = \frac{\ln\left(\frac{t}{t_0}\right)}{c} \tag{1}$$

Herein, t is the sample flow time, t_0 is the solvent flow time (NMP/LiCl), and c is the sample concentration. ^{1}H NMR spectra were recorded on a Bruker Avance 400 MHz spectrometer using DMAc-d9 solutions of the telechelics and block copolymers.

Thermal Analysis (Differential Scanning Calorimetry)

Differential Scanning Calorimetry (DSC) was used to determine the glass transition temperature (T_g) of the telechelics and polymers. Measurements were run in nitrogen atmosphere on a TA Instruments DSC Q2000 using the following temperature profile: Ramp from 40 °C to 450 °C at 10 °C/min, isothermal for 10 min, ramp to 40 °C at 10 °C/min, isothermal for 5 min, ramp to 450 °C at 10 °C/min. The second heating cycle was used for data analysis.

Preparation of PBI Membranes and PBI-H_3PO_4 Complexes

Membranes were prepared by solution casting from NMP/LiCl (1 wt % LiCl). The block copolymers were dissolved in NMP/LiCl (11–14 wt % block copolymer concentration depending on the block length ratio) at 95 °C (ca. 2 h). These solutions were cast onto glass plates using a doctor blade with a gate thickness of 20 mils. The glass plates were transferred into a preheated vacuum oven (80 °C). Then, vacuum was set to about 14 inch Hg while temperature was increased to 140 °C within 2 h. Finally, the vacuum was reduced to 1 inch Hg for another 2 h. The membranes were post-treated in distilled water at 95 °C for 24 h to remove residual solvent. After drying the membranes at 130 °C in vacuo (1 inch Hg), they were immersed in phosphoric acid at room temperature for 48 h to form the membrane H_3PO_4 complexes.

Membrane Characterization and Fuel Cell Testing

Liquid and Weight Uptakes

At least three samples of membrane H_3PO_4 complexes (size 2 cm × 3 cm) were prepared, blotted with filter paper and weighed. Each sample was placed in 50 mL distilled water and allowed to stir at 95 °C for at least 20 min. After cooling to room temperature, the samples were titrated with 0.1 M sodium hydroxide solution ($c = 0.1$ M) using a Metrohm 716 DMS Titrino titrator. The first equivalence point was used to determine the volume of sodium hydroxide (V). Then, the membrane samples were washed thoroughly with distilled water and dried in a vacuum oven at 130 °C for 16 h. The samples were cooled to room temperature under vacuum and weighed again (w_1). The following set of values can then be calculated with the weight of the wet membrane (w_2), of the dry membrane (w_1), the concentration (c), the volume of sodium hydroxide solution (V), and the molar mass of phosphoric acid (M)

Acid weight [%]:

$$w_A = \frac{M \cdot V \cdot c}{w_2} \cdot 100 \tag{2}$$

Water Weight [%]:

$$w_W = \frac{(w_2 - w_1) - M \cdot V \cdot c}{w_2} \cdot 100 \tag{3}$$

Polymer Weight [%]:

$$w_P = \frac{w_1}{w_2} \cdot 100 \tag{4}$$

Liquid Uptake and Swelling Degree

Non-doped membrane pieces (3.5 cm × 7 cm) were dried at 130 °C in a vacuum oven for 16 h and their actual length ($l_{x,1}$), width ($l_{y,1}$), thickness ($l_{z,1}$), and weight (w_1) were determined (l_y refers to the casting direction of the membrane, l_x perpendicular to casting direction). Then, the membranes were equilibrated in phosphoric acid for 48 h. Then, they were blotted with filter paper and their dimensions and weights were recorded again ($l_{x,2}$, $l_{y,2}$, $l_{z,2}$, w_2). The liquid uptake and swelling degree were calculated using the following equations.

$$\text{Liquid uptake} = \frac{w_2 - w_1}{w_1} \cdot 100 \tag{5}$$

$$\text{Swelling degree} = \frac{l_2 - l_1}{l_1} \cdot 100 \tag{6}$$

TABLE 1 Overview of Properties for the Series of Telechelic PBI Macromonomers

Name	M_n^{target} (kDa)	IV (dL/g)	T_g (°C)
PBI-5	5	0.93	419
PBI-7.5	7.5	1.08	427
PBI-10	10	1.51	428
PBI-15	15	1.74	432
homo-PBI	∞	1.92	-

Proton Conductivity and Mechanical Properties

Proton conductivities were measured by a four-probe electrochemical impedance spectroscopy method using a Zahner IM6e electrochemical workstation over the frequency range from 1 Hz to 100 kHz with amplitude of 5 mV. The conductivities of the membranes were calculated as follows:

$$\sigma = \frac{d}{l \cdot b \cdot R_m} \quad (7)$$

where d is the distance between the two inner probes, l is the thickness of the membrane, b is the width of the membrane, and R_m is the ohmic resistance from the model fitting.

The mechanical properties of the membranes were tested on an Instron 5543A tensile tester with a 22.2 N load cell. Samples were cut following the ASTM standard D 683 (Type V specimens) and measured in air atmosphere at room temperature.

Membrane Electrode Assembly Fabrication and Fuel Cell Testing

Membrane electrode assemblies (MEAs) were fabricated by hot-pressing a sandwich consisting of doped membrane pieces (typical thicknesses 80–150 microns) and two gas diffusion electrodes (cathode: ELAT 3480, 1 mg/cm^2 Pt alloy; anode: ELAT 3570, 1 mg/cm^2 Pt) at 140 °C for 30 s on a manual Carver press. The active area of MEA was 44 cm^2, and it was assembled into a single fuel cell testing fixture and tested as described previously.[32] For the modified electrode preparation, dry 6F-PBI powders were dissolved in DMAc (0.5 wt %). The PBI/DMAc solution was sprayed onto BASF standard electrodes with an air brush (Badger, air brush model 100). The electrodes were dried in a vacuum oven (ca. 30 inch Hg, 120 °C) overnight. The 6F-PBI loading was 0.1 mg/cm^2. MEAs were subjected to a break-in period by running cells at 160 °C for 24–48 h in hydrogen/air ($\lambda(H_2) = 1.2$ and $\lambda(air) = 2.0$ stoichiometry, no humidification) at atmospheric pressure. Polarization curves were run at 160 °C with identical gases, pressures, and stoichiometry using flow tracking software.

RESULTS AND DISCUSSION

Characterization of Telechelic PBI Macromonomers

Various block lengths of telechelic PBI macromonomers were synthesized using appropriate stoichiometric imbalance of the corresponding monomers (PBI-x with $x = 5$, 7.5, 10, 15). As a reference, polymeric PBI was produced using the stoichiometric ratio of 1 (PBI). The characterization results are summarized in Table 1. As expected, both the intrinsic viscosity and the glass transition temperature (T_g) increase with increasing block length.[33] T_g for the polymeric PBI could not be found experimentally. However, when using the Flory–Fox equation for plotting the T_g values for the telechelics,[34] the calculated T_g of the polymeric PBI would be 438 °C which closely matches the values reported in the literature (420 °C–450 °C).[35–38]

Characterization of Carboxyl End-Capped Poly(Arylene Ether) Macromonomers

The non-PBI telechelics were characterized with the same methods as the PBI telechelics, and the results are summarized in Table 2. Due to the relatively high flexibility of the ether bridge, the intrinsic viscosity and glass transition temperatures are relatively low compared to the rigid polybenzimidazole telechelics, but are in a typical range for poly(arylene ether)s.[39] We found, for example, 0.19 dL/g for the telechelic PAEPO-5 (measured in NMP/LiCl) and determined T_g to be 236 °C. In the literature, values for homo-PAEPO are reported to be IV = 0.33 dL/g (in CH_2Cl_2) and $T_g = 240$ °C. Considering the lower molecular weight of the PAEPO-5 reported here, the values are consistent with the literature.[40]

Characterization of Poly(Arylene Ether)-*Block-Meta*-Polybenzimidazoles

A focus of this work was to prepare, characterize, and compare the properties of different block copolymers as membrane materials in high-temperature membrane fuel cells. Herein, the chemical and thermal properties of the block copolymers resulting from the combination of telechelic polybenzimidazoles with various telechelic poly(arylene ether)-based macromonomers are discussed. In particular are considered, (i) the influence of block length variations of non-PBI to PBI segments, and (ii) the influence of the chemical structure in the non-PBI segments while the PBI segment is kept constant.

Table 3 summarizes the intrinsic viscosities (IVs) for variations in the block length ratio. When the non-PBI telechelic was kept constant at 5 kDa (fPAE-5) and the PBI block length was increased from 5 to 15 kDa, the IV increased in

TABLE 2 Overview of Properties for the Series of Carboxyl End-Capped Poly(Arylene Ether) Macromonomers

Name	M_n^{target} (kDa)	IV (dL/g)	T_g (°C)
fPAE-5	5	0.13	200
fPAE-10	10	0.15	201
fPAES-5	5	0.20	-
PAES-5	5	0.28	212
PAEPO-5	5	0.20	236

TABLE 3 IVs of the Condensation Products Between PBI and the Partially Fluorinated Non-PBI Telechelics

Name	IV Block Copolymer (dL/g)	IV PBI Telechelics (dL/g)	IV Non-PBI Telechelics (dL/g)
PBI-5/fPAE-5	0.76	0.93	0.13
PBI-7.5/fPAE-5	1.37[a]	1.08	0.13
PBI-10/fPAE-5	1.28	1.52	0.13
PBI-15/fPAE-5	1.65	1.77	0.13
PBI-10/fPAE-10	1.12[a]	1.43	0.15
homo-PBI	1.82		

[a] Polymer could not be dissolved completely; some gel particles were observed.

the same order from 0.76 to 1.65 dL/g, but with the exception of PBI-7.5/fPAE-5 that might have reached a higher polymerization degree in the coupling reaction compared to the others (this is also supported by the presence of gel particles). The IVs of the final block copolymers were lower (except for PBI-7.5/fPAE-5) than those of the corresponding PBI telechelics. This is understandable as the hydrodynamic behavior of the block copolymers in solution depends not only on the molecular weight of the polymer but also on its flexibility. The latter was highly increased in the block copolymer due to the poly(aryl ether) segments. The same behavior was observed when the block length of the non-PBI segment was increased (cf. PBI-10/fPAE-10).

Table 4 shows the IVs for the block copolymers made from 10 kDa PBI telechelics and the various 5 kDa non-PBI telechelics. Only PBI-10/PEAPO-5 shows an increase in IV compared to that of the PBI telechelics which is, most likely, due to the lower flexibility of the bulky phenyl phosphine oxide linkage group in the backbone.

Unlike the individual PBI and non-PBI telechelics, the block copolymers did not show any evidence for glass transition temperatures in the DSC. One would have expected to detect either two glass transition temperatures in the block copolymers (in case of non-miscible polymers) at the position of the individual telechelics or one glass transition at a mean position between the two individual telechelics (in case of miscible polymers).[41] Multiple scanning rates also did not reveal glass transition temperatures.

^{1}H NMR spectroscopy was used to detect the presence of reactive end groups in the telechelic macromonomers and the successful coupling reaction to the respective block copolymers. As an example, Figure 3 shows the spectra of the telechelic macromonomers fPAE-5 and PBI-10 together with the spectrum of the corresponding block copolymer PBI-10/fPAE-5. The small peaks of the fPAE-5 and PBI-10 spectra could be assigned to hydrogen nuclei of their reactive carboxyl and diaminobenzidine end groups. Quantitative end group analysis was representatively made for these two telechelics: 4.7 kDa was obtained for fPAE-5 which is very close to the expected value of 5.0 kDa showing that controlling the molecular weight by the stoichiometry of monomers was successful. The analysis of the PBI-10 spectrum yielded a range of 11.0 to 15.7 kDa depending on the integration mode, within expectations for the synthetic conditions used in this study. The NMR spectrum of PBI-10/fPAE-5 revealed the successful coupling between the PBI and non-PBI telechelics. As the mobility of the polymer backbone is much more restricted in high-viscous media, the broadening of the peaks is a first indication that a high-molecular weight polymer was formed. The peaks of the reactive former end groups disappear as well and the signals 1 and 2 in the fPAE-5 block were shifted to lower field according to expectations. The signal at around 9.45 ppm was assigned to nucleus 3 in the fPAE-5 segments after coupling. Perhaps the most striking evidence for coupling of the non-PBI and m-PBI blocks was the change in the physical appearance of the materials. Low molecular precursors (both PBI and non-PBI) appeared as friable powders, where the successfully coupled block copolymers formed strong, coherent films (Supporting Information Fig. S1).

Membrane Characterization

Relationship between Doping Level and Conductivity

Figure 4 shows the liquid uptake of the series of membranes containing various ratios of PBI to fPAE telechelics in comparison to *homo*-PBI. Phosphoric acid concentrations below 9 M H_3PO_4 yielded liquid uptakes lower than 150% which appears very low for achieving proton conductivities in the range necessary for fuel cell applications. The membranes with the same ratios of PBI and non-PBI segments (PBI-10/fPAE-10 and PBI-5/fPAE-5) and with block lengths of PBI $\leq$ 7.5 kDa also had low values for liquid uptake in 12 M phosphoric acid. The highest liquid uptakes in 12 M H_3PO_4 were found in membranes of *homo*-PBI and the block copolymer with the highest PBI/non-PBI ratio (PBI-15/fPAE-5). Specific proton conductivities of these membranes were compared after doping in 12 M and 14.6 M phosphoric acid (cf. Fig. 5) to determine a suitable doping procedure for the new block copolymer membranes. It is generally accepted that the proton conductivity of a fuel cell membrane should be 0.1 S/cm or greater at operational conditions.[42]

The proton conductivities of PBI-15/fPAE-5 block copolymer and the *homo*-PBI reference membranes were only 0.016 S/cm and 0.024 S/cm at 180 °C when doped in 12 M H_3PO_4. When

TABLE 4 IVs of the Condensation Products Between PBI and the Various Non-PBI Telechelics

Name	IV Block Copolymer (dL/g)	IV PBI Telechelics (dL/g)	IV Non-PBI Telechelics (dL/g)
PBI-10/fPAE-5	1.28	1.52	0.13
PBI-10/fPAES-5	1.35	1.36	0.20
PBI-10/PAES-5	1.35	1.52	0.28
PBI-10/PAEPO-5	1.36	1.36	0.19

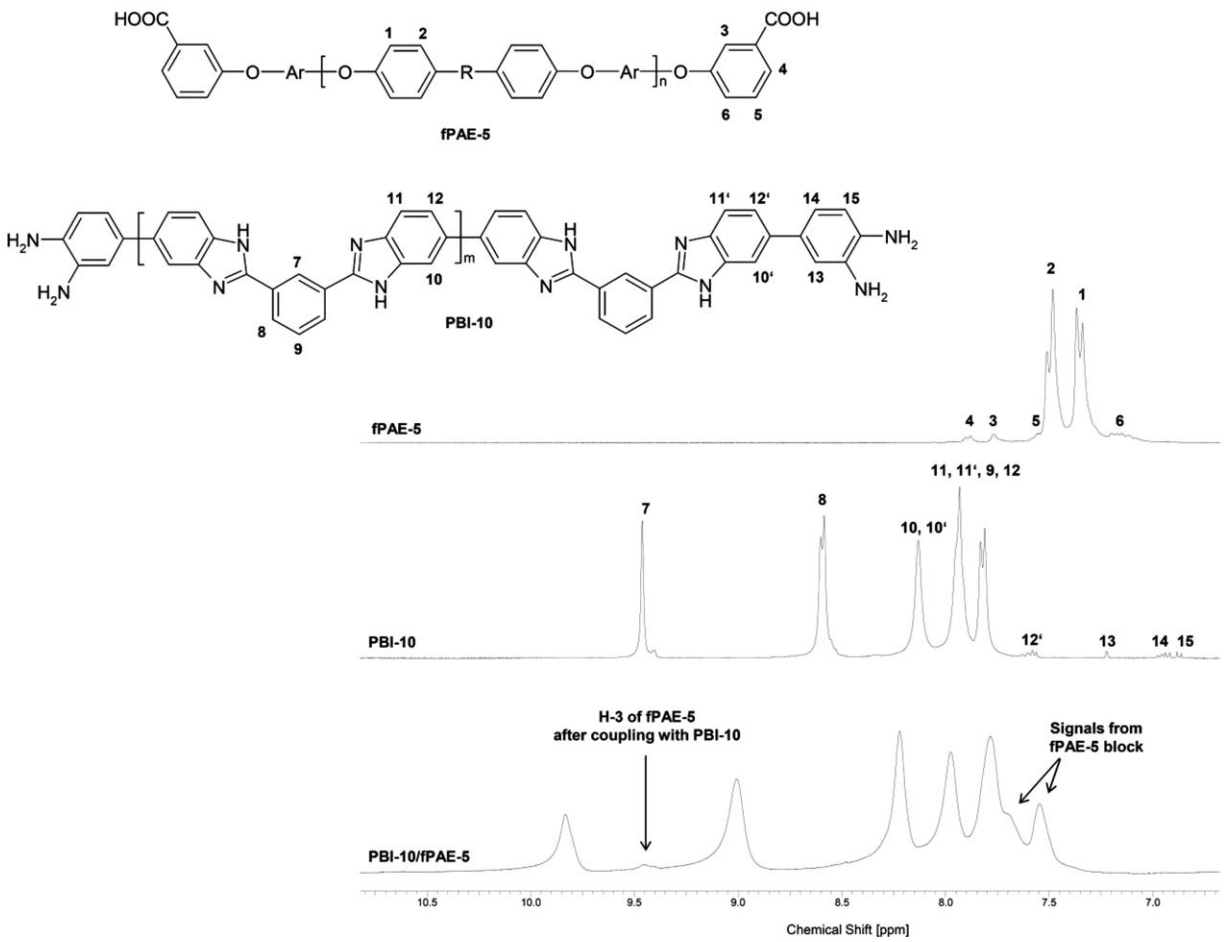

FIGURE 3 ^{1}H NMR spectra of the telechelic macromonomers fPAE-5, PBI-10, and the corresponding block copolymers PBI-10/fPAE-5.

the same membranes were doped in 14.6 M H_3PO_4, the proton conductivity increased by a factor of about 5 (0.108 S/cm and 0.127 S/cm at 180 °C). Therefore, phosphoric acid with a concentration of 14.6 M was used for membrane doping of the series of new block copolymers.

Influence of the Block Lengths and Block Length Ratio on Ex Situ Properties

A series of block copolymers consisting of a 5 kDa partially fluorinated poly(arylene ether) (fPAE-5) and various lengths of PBI blocks ($x = 5$, 7.5, 10, 15 kDa) was compared to *homo*-PBI in terms of their liquid uptake, membrane swelling, and ionic conductivities. In addition, another block copolymer with 10 kDa blocks in both the phosphophobic and phosphophilic block was directly compared to investigate the influence of individual block lengths.

Figure 6 shows the liquid uptake of the various membranes, including *homo*-PBI, plotted as the mole fraction of PBI in the copolymer. The solid line was calculated based on the experimental value of liquid uptake for *homo*-PBI weighted by the mole fraction of the PBI component of the block copolymers. The measured liquid uptake for PBI-5/fPAE-5 (228%) and PBI-10/fPAE-10 (171%) is very close to those reported by McGrath et al. for similar 1: 1 (PBI: non-PBI) systems. They reported 200% for their PBI-5/Non-PBI-5 and 180% for their PBI-10/Non-PBI-10 block copolymer.[21] In the current series of block copolymers with 5 kDa fPAE, the experimentally measured values for liquid uptake followed a linear correlation with PBI content. This suggests that the

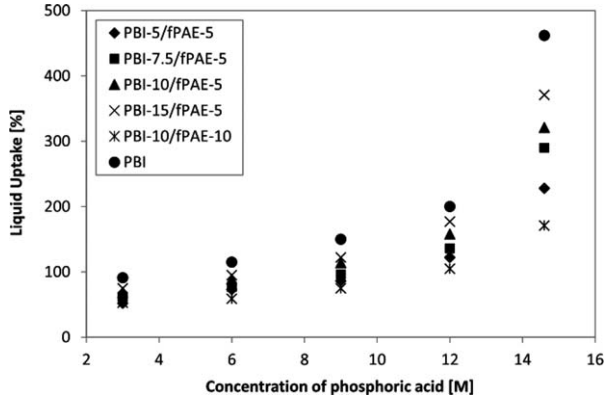

FIGURE 4 Liquid uptake of block copolymer membranes with variation in block length in comparison to *homo*-PBI membranes.

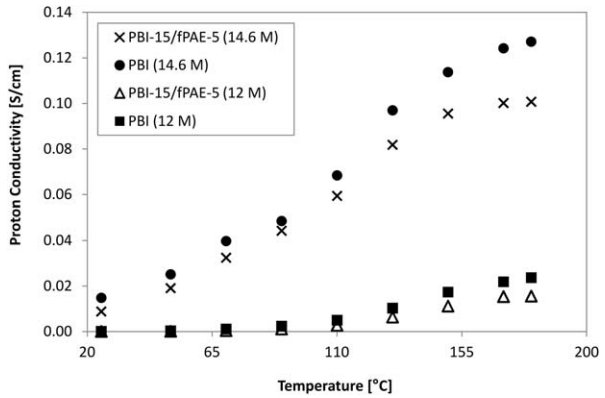

FIGURE 5 Conductivity of membranes made of acid-doped *homo*-PBI and PBI-15/fPAE-5 block copolymer. Different phosphoric acid concentrations [12 M vs. 14.6 M] were used for the doping process.

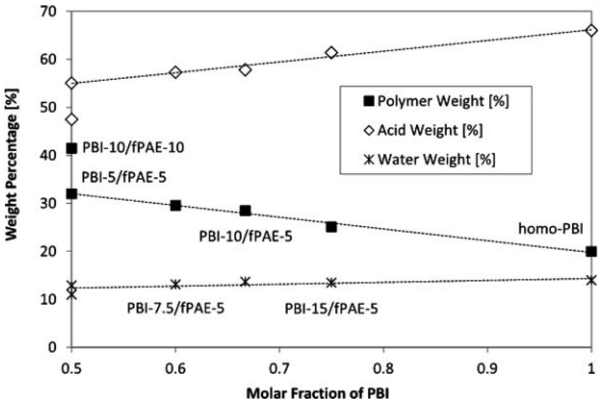

FIGURE 7 Polymer, acid, and water distribution of the membrane-phosphoric acid complexes.

non-PBI domains do not interact with phosphoric acid and that the PBI domains in the block copolymers have the same interaction mode as *homo*-PBI. The sample with larger PBI blocks (PBI-10/fPAE-10) deviates from this pattern. Its liquid uptake was about 50% less than that of PBI-5/fPAE-5 and less than expected on the basis of the calculation. This might indicate changes in morphology that significantly alter membrane properties.

The distribution of polymer, acid, and water in the membrane-phosphoric acid complexes was determined by titration and is summarized in Figure 7. A similar trend for the copolymers with 5 kDa fPAE blocks was observed as discussed above for the total liquid uptake. The acid weight percentage in the membrane increased with increasing mole fraction of PBI in the copolymer and accordingly, the opposite trend was observed for the polymer weight percentage. It should be noticed that the water content was not affected by the composition and was the same for all block copolymers. When comparing the degree of swelling of the block copolymers, higher deviations from the calculated values based on PBI mole fraction were observed (Fig. 8).

Although the block copolymers with 5 kDa fPAE blocks showed a significantly lower liquid uptake, the swelling in both the *z*-direction and *x,y*-plane was considerably higher than the calculations, based on PBI mole fraction. Remarkably, the degree of swelling in the *x,y*-plane exceeded that for *homo*-PBI when the block length was higher than 10 kDa. While the liquid uptake of the block copolymers per PBI repeating unit was the same in the *homo*-PBI, the dimensional changes were much higher which may be due to the strong repulsion of the non-PBI and H_3PO_4-PBI domains. As expected from the liquid uptake, the PBI-10/fPAE-10 block copolymer showed lower dimensional changes in H_3PO_4. In contrast to McGrath's findings that the dimensional change in length of 1:1 (PBI:non-PBI) block copolymers could be reduced by factor 8, our PBI/fPAE system showed a less pronounced effect. For example, the swelling in the *z*-direction for PBI-10/fPAE-10 could only be reduced by about 3 when compared with PBI (Fig. 8). This less pronounced reduction of swelling might be a consequence of the morphological difference that arises from the different chemical structure of the PBI segments. The higher swelling values in the *x,y*-plane of PBI-10/fPAE-5 and PBI-15/fPAE-5 compared to *homo*-PBI also suggest that the swelling behavior is quite complex and

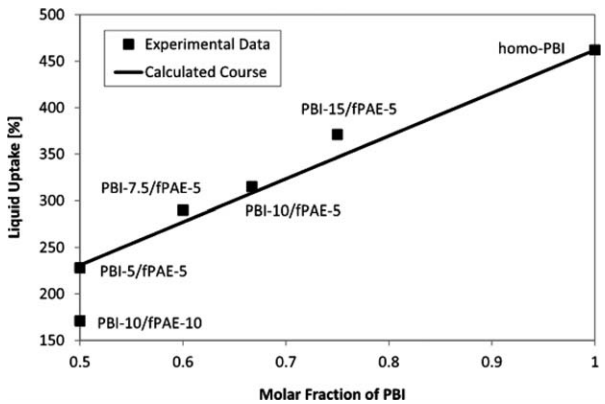

FIGURE 6 Liquid uptake of different block copolymers and *homo*-PBI in concentrated phosphoric acid (14.6 M) at room temperature.

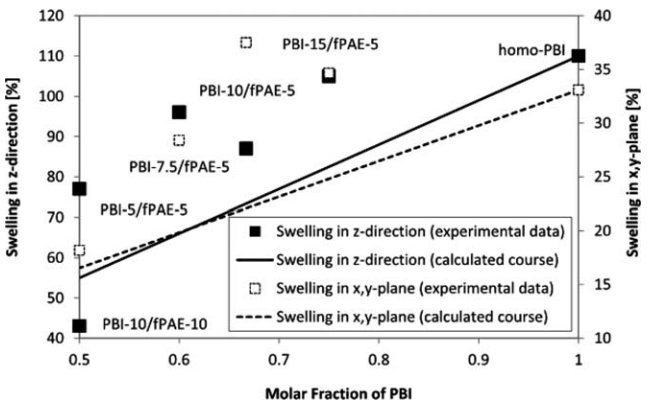

FIGURE 8 Swelling behavior of different block copolymers and *homo*-PBI in concentrated phosphoric acid at room temperature.

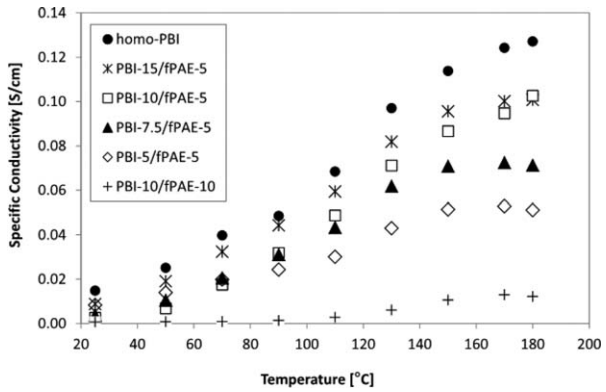

FIGURE 9 Effects of block lengths on the specific conductivities of the block copolymers.

probably dependent on multiple factors such as block chemistries, block lengths, processing conditions, and so forth.

Specific conductivities of the membrane-phosphoric acid complexes were determined by electrochemical impedance spectroscopy at temperatures up to 180 °C (Fig. 9).

The specific conductivity increased with temperature and with increasing length of PBI blocks from about 0.05 S/cm for PBI-5/fPAE-5 to 0.1 S/cm for PBI-10/fPAE-5 and PBI-15/fPAE-5, respectively. PBI-10/fPAE-10 displayed very low proton conductivity, and, was therefore not further evaluated. Figure 10 shows the specific conductivity at 180 °C per percent of phosphoric acid, and indicates the effectiveness of the phosphoric acid to the proton migration mechanism. This value shows a maximum at the composition PBI-10/fPAE-5. Although the specific conductivity of PBI-15/fPAE-5 was similar to PBI-10/fPAE-5, the utilization of phosphoric acid appears to be more effective for PBI-10/fPAE-5. Therefore, this composition was chosen for further investigation of the electrochemical behavior in an MEA (see Fuel cell performance section).

In addition to the liquid uptake, swelling behavior, and specific conductivity, the mechanical properties of acid-doped

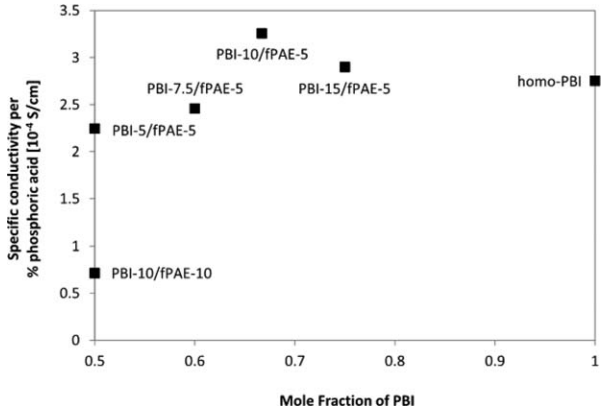

FIGURE 10 Specific conductivity of the block copolymers and of *homo*-PBI at 180 °C related to the percentage of liquid uptake.

TABLE 5 Comparison of Important Mechanical Properties of Phosphoric Acid Doped Block Copolymer Membranes in Comparison to *Homo*-PBI Membranes

Name	Liquid Uptake (%)	Modulus (MPa)	Tensile Strength (MPa)	Elongation at Break (%)
PBI-5/fPAE-5	228	34.6 ±4.1	7.0 ± 1.8	9.4 ± 1.2
PBI-10/fPAE-5	315	17.8 ± 3.1	12.2 ± 1.0	13.6 ± 1.9
PBI-15/fPAE-5	371	9.4 ± 1.3	14.7 ± 1.8	27.1 ± 3.4
PBI-10/fPAE-10	171	24.3 ± 5.7	15.0 ± 2.7	14.1 ± 2.7
homo-PBI	462	6.7 ± 2.9	14.3 ± 6.2	33.6 ± 15.9

membranes are important parameters for their intended use in an MEA. Table 5 gives an overview of the mechanical properties of the new block copolymers compared to *homo*-PBI membranes. Within the series from *homo*-PBI, PBI-15/fPAE-5 to PBI-5/fPAE-5, the modulus increased with decreasing mole fraction of PBI. This is a likely consequence of the lower plasticizer content (H_3PO_4) and the reinforcing effect of the non-PBI domains.

Liquid Uptake and Swelling Behavior

As shown in Figure 2, the chemical structure in the non-PBI block was varied while the ratio between PBI and non-PBI segments remained constant. The resulting *ex situ* properties were compared to aid the selection of the most-promising candidate from this series for *in situ* fuel cell testing. The liquid uptake and swelling behavior for this series is shown in Table 6. PBI-10/PAEPO-5 showed similar liquid uptake values as *homo*-PBI, but higher degrees of swelling in both the *z*-direction and in the *x*,*y*-plane. This behavior can be explained by the capability of the phosphine oxide groups in the non-PBI domains to interact with phosphoric acid. The relatively bulky phenyl substituents might also contribute to the higher dimensional change during the doping procedure. In contrast to the phosphine oxide bridged block copolymer, the liquid uptake of the three other structures (fPAE, PAES, and fPAES) was significantly lower. The swelling in the *z*-direction was significantly lower than that for *homo*-PBI and PBI-10/PAEPO-5, but the swelling in the *x*,*y*-plane was in the same range as the others. This difference is most likely due to the lower liquid uptake although the polymer structure

TABLE 6 Liquid Uptake and Swelling of *Homo*-PBI and the Block Copolymers with Various Chemical Structures in the Non-PBI Block

Name	Liquid Uptake (%)	Swelling in *z*-Direction (%)	Swelling in *x*,*y*-Direction (%)
homo-PBI	462	110	33
PBI-10/fPAE-5	315	63	38
PBI-10/PAES-5	238	65	28
PBI-10/fPAES-5	286	60	31
PBI-10/PAEPO-5	445	126	38

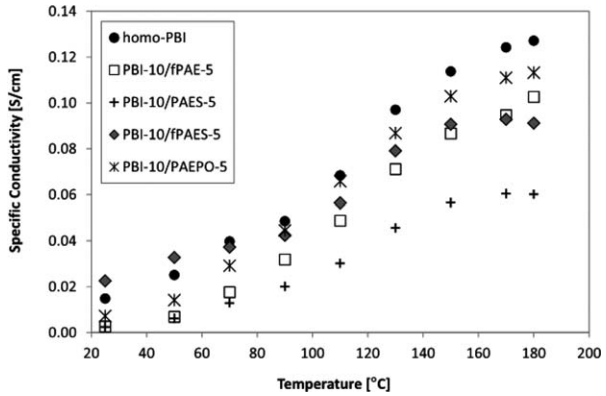

FIGURE 11 Specific conductivities of the block copolymers with various chemical structures in the non-PBI block in dependence of temperature.

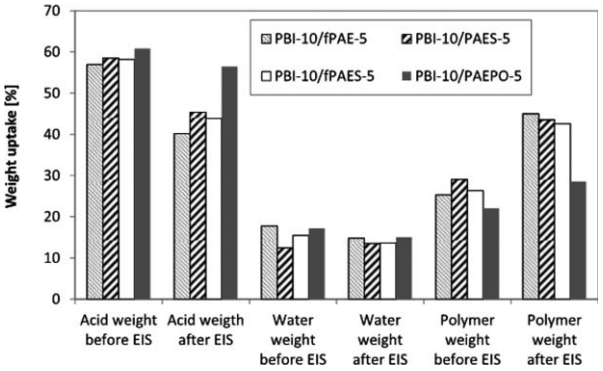

FIGURE 13 Weight distribution of acid, water, and polymer of the doped membranes before and after electrochemical impedance spectroscopy.

and morphology may play an important role as well. However, in this empirical and comparative study, we were evaluating the principal applicability of block copolymers as fuel cell membranes. In this context, the specific proton conductivity of the various membrane materials is very important.

Figure 11 shows the temperature dependence of the proton conductivity for these membrane-H_3PO_4 complexes. PBI-10/PAES-5 showed a proton conductivity of only 0.06 S/cm at 180 °C while PBI-10/fPAES-5 was about 0.09 S/cm at 180 °C. This difference was attributed to the slightly higher liquid uptake (48%) in combination with the structural difference in the non-PBI block. However, the proton conductivity of PBI-10/fPAES-5 reached a maximum at 170 °C and showed a slight decrease at higher temperatures. McGrath et al. also synthesized block copolymer structures with PAES structures.[21] As mentioned in the introduction, they kept the PBI to PAES ratio the same, and focused on three block copolymers (PBI-5/PAES-5, PBI-10/PAES-10, PBI-15/PAES-15) and measured proton conductivities in the range of 0.032 to 0.042 S/cm at 180 °C. In the current study the block length ratio of PBI to PAES was increased to reach higher proton conductivities, and thus the measured values are in the expected range. The proton conductivities of PBI-10/PAEPO-5 and PBI-10/fPAE-5 were slightly lower than those measured for *homo*-PBI, but in the targeted range of 0.1 S/cm at 180 °C. Since the proton conductivities of PBI-10/PAEPO-5 and PBI-10/fPAE-5 were in the same range, but the liquid uptake was considerably different (445% vs. 315%), different morphological structures of these block copolymer membranes are likely (the chain lengths of the domains are comparable, cf. Table 2). The weight percentages of polymer, acid and water were compared for the new block copolymers with different chemical structure in the non-PBI segments in Figure 12. Compared to *homo*-PBI, all block copolymers showed lower acid and higher polymer percentages, as expected. While the water content of PBI-10/fPAE-5 and PBI-10/PAES-5 were about the same as for *homo*-PBI, PBI-10/fPAES-5, and PBI-10/PAEPO-5 absorbed more water.

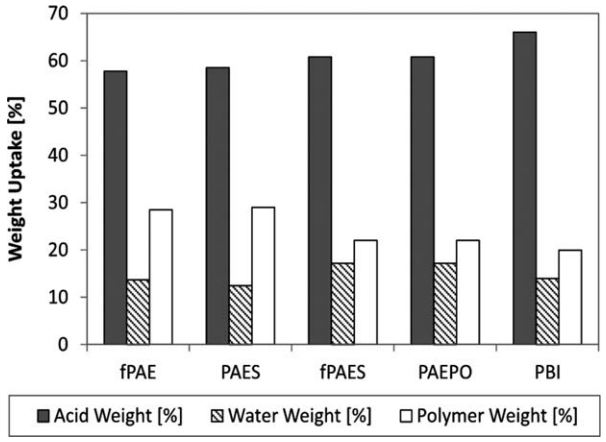

FIGURE 12 Weight distribution of acid, water, and polymer of the doped membranes before electrochemical impedance spectroscopy.

To estimate the compositional stability of the polymer-H_3PO_4 complexes and the binding capacity toward H_3PO_4 specifically, the membrane H_3PO_4 complexes were titrated before and after conductivity measurements (cf. Fig. 13). All membranes lost phosphoric acid, whereas the effect was less pronounced for PBI-10/PAEPO-5. Phosphoric acid loss is one of the well-recognized degradation phenomena in PBI/H_3PO_4-based fuel cells.[43] Since the *ex situ* characteristics cannot be transferred directly to an operating fuel cell, one membrane (PBI-10/fPAE-5) from this series was selected for detailed *in situ* fuel cell testing based on a favorable balance of properties (overall conductivity, conductivity per acid content, mechanical properties, and swelling behavior).

Mechanical data for this series show similar trends as discussed earlier (cf. Table 7). With the exception of PBI-10/PAEPO-5, all of the copolymers displayed a higher modulus than *homo*-PBI and correlates with the lower phosphoric acid loadings in the membranes.

Fuel Cell Performance

Ex situ characterization of fuel cell membranes can only serve as a tool for the pre-selection of membranes that, in principle, are suitable in fuel cells. Unfortunately, no

TABLE 7 Comparison of Important Mechanical Properties of Phosphoric Acid Doped Block Copolymer Membranes in Comparison to *Homo*-PBI Membranes

Name	Liquid Uptake (%)	Modulus (MPa)	Tensile Strength (MPa)	Elongation at Break (%)
homo-PBI	462	6.7 ± 2.9	14.3 ± 6.2	33.6 ± 15.9
PBI-10/fPAE-5	315	17.8 ± 3.1	12.2 ± 1.0	13.6 ± 1.9
PBI-10/PAES-5	238	16.8 ± 8.5	9.5 ± 2.6	16.8 ± 6.6
PBI-10/fPAES-5	286	12.5 ± 1.9	10.5 ± 2.9	17.6 ± 6.3
PBI-10/PAEPO-5	445	4.1 ± 0.8	9.7 ± 0.8	34.5 ± 4.3

previous *in situ* fuel cell data for PBI-based block copolymers could be found in the literature. To fill this gap in the literature and to estimate the potential of such materials as alternative membranes, the *in situ* characterization of the preselected membrane PBI-10/fPAE-5 was performed. Polarization curves of the new block copolymer membrane are shown in Figure 14 with comparison to *homo*-PBI membrane. All MEAs were prepared under the same conditions using standard electrodes and standard pressing parameters.

As shown in Figure 14, the OCV of the membrane was approximately the same as the *homo*-PBI membrane, which demonstrates the integrity of the block PBI membrane at the operational temperature. The MEA resistance (the slope of the linear part of the polarization curve) of the block PBI membrane was much higher than the *homo*-PBI membrane. The MEA resistance mainly consists of the membrane resistance, electrode resistance, and membrane/electrode resistance. The block PBI membrane had similar thickness and proton conductivity as the *homo*-PBI membrane, so the membrane resistances were approximately the same. Since identical electrodes were used, the difference between the MEA resistances was thus attributed to the differences in the membrane/electrode interfacial resistances. We speculated that the higher interfacial resistance of the block PBI membrane/electrode could be due to either the lack of phosphoric acid at the interface or the incompatibility of the block copolymer membrane with the electrode. Figures 15 and 16 show the time-dependent fuel cell performances of the membranes at 160 °C in H_2/air with gas stoichiometries of $\lambda(H_2) = 1.2$ and $\lambda(\text{air}) = 0.2$). For *homo*-PBI, constant operation at 0.2 A/cm^2 was possible while the block copolymer membranes could only be operated at 0.05 A/cm^2. Polarization curves were recorded after a short break-in time, and for PBI-10/fPAE-5, also after 404 h of operation at 0.05 A/cm^2. It can clearly be seen that the fuel cell performance of the block copolymer membrane was considerably lower than the reference *homo*-PBI membrane. There was a breakdown of the test station for the PBI-10/fPAE-5-based MEA at 155 h (Fig. 16); after restarting the test, the voltage stabilized after another 100 h to approximately 20–30 mV lower than the initial value. After recording polarization curves, the voltage increased slightly. However, the achieved power density was too low for real fuel cell applications and was incapable of sustaining a load above approximately 0.05 A/cm^2. All of the other block copolymer membranes showed similar low fuel cell performances. Two approaches were examined to solve the membrane/electrode interface issue. A recently described acid/membrane pretreatment method was adapted to add more phosphoric acid at the interface of the membrane/electrode.[44] However, this

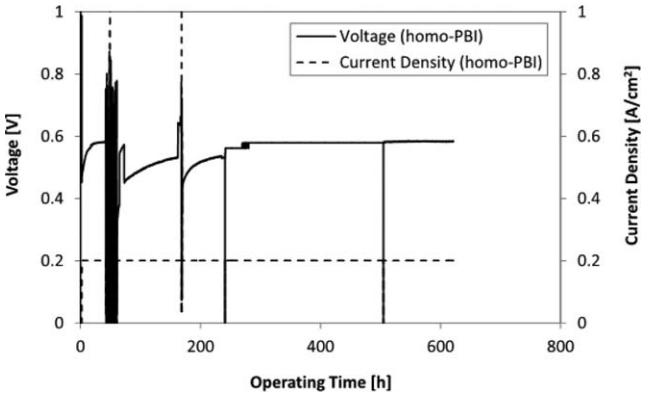

FIGURE 15 Durability testing of *homo*-PBI membranes at 0.2 A/cm^2 at 160 °C.

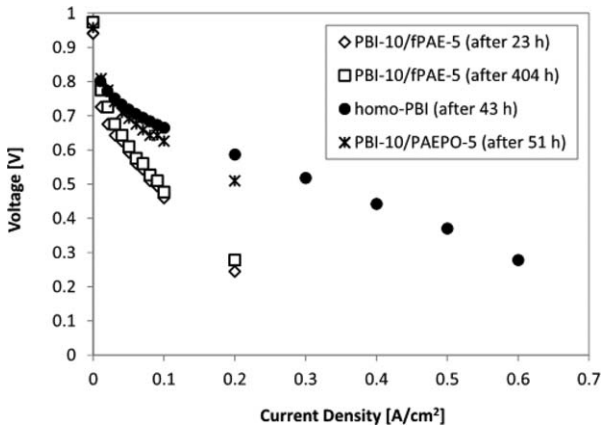

FIGURE 14 Polarization curves of MEAs at 160 °C in H_2/air with $\lambda(H_2) = 1.2$ and $\lambda(\text{air}) = 2.0$.

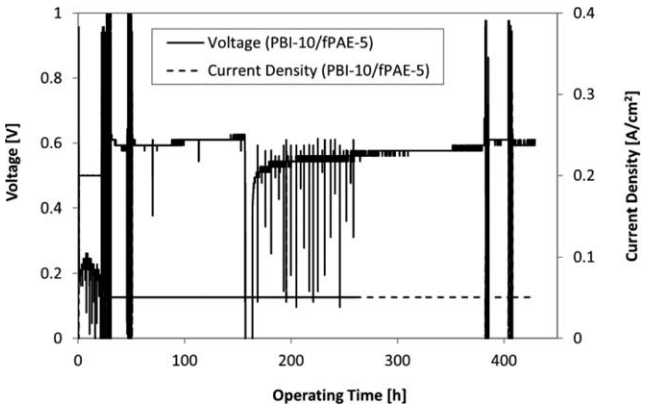

FIGURE 16 Durability testing of PBI-10/fPAE-5 membrane at 0.05 A/cm^2 at 160 °C.

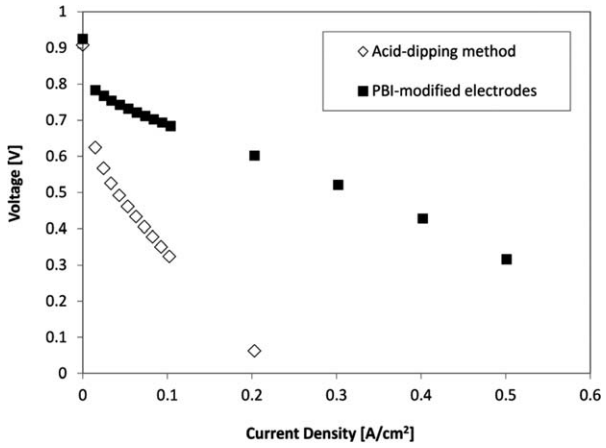

FIGURE 17 Polarization curves of PBI-10/fPAE-5 membrane at 160 °C in H2/air with gas stoichiometries of $\lambda(H_2) = 1.2$ and $\lambda(\text{air}) = 2.0$ (atmospheric pressure with no back pressure).

method did not improve the fuel cell performance of the block copolymer membrane as shown in Figure 17.

PBI modified electrodes (with 0.1 mg/cm^2 added 6F-PBI to the electrode surfaces) were used to resolve the incompatibility between the block copolymer and electrodes with much improved results. The polarization curve is shown in Figure 17, and the time-dependent fuel cell performance is shown in Figure 18. The MEA resistance of the block copolymer PBI membrane was noticeably decreased and showed a dramatic improvement of membrane/electrode interface with the introduction of 6F-PBI polymer at the surface of electrodes. The fuel cell with a block copolymer PBI membrane was constantly operated at 0.2 A/cm^2 over 2000 h with an initial 0.58V at 0.2 A/cm^2 and approximately 20 μV/h performance degradation rate, which are both similar to the *homo*-PBI membrane. We contend that the absence of fuel cell data on previously reported PBI-based block copolymer membranes may be a result of the poor interface with standard electrodes. Future studies should be greatly enhanced by the approach reported herein.

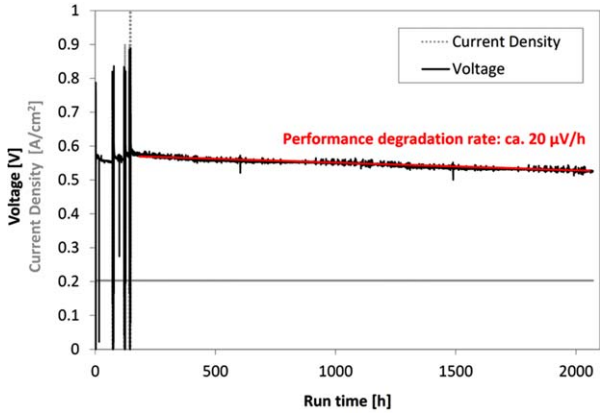

FIGURE 18 Durability testing of PBI-10/fPAE-5 membrane with 6F-PBI modified electrodes at 0.2 A/cm^2 at 180 °C in H_2/air with gas stoichiometries of $\lambda(H_2) = 1.2$ and $\lambda(\text{air}) = 2.0$ (atmospheric pressure with no back pressure). [Color figure can be viewed at wileyonlinelibrary.com]

CONCLUSIONS

We report the first fuel cell testing for acid doped block copolymers consisting of PBI and non-PBI segments. The targeted block copolymers could be synthesized and made into H_3PO_4-doped membranes with reasonable mechanical properties. *Ex situ* characterization demonstrated that control of the block copolymer chemistry and block lengths can lead to membranes with an improved balance of properties including PA doping levels and ionic conductivity needed in fuel cells. However, the initial *in situ* electrochemical characterization revealed that these block copolymers performed poorly in fuel cells compared to previous reports of membrane compositions with comparable PA loadings and ionic conductivities and were incapable of sustaining loads much above 0.05 A/cm^2.

The poor interfaces between the block copolymer membranes and the electrodes (designed for membranes with different structures) were suspected to be the cause of the poor performance and two approaches were investigated to enhance the fuel cell performance.

A successful approach was identified and tested that involved the pretreatment of the electrodes with a fluorinated 6F-PBI prior to MEA fabrication. This treatment dramatically improved the electrochemical characteristics of fuel cells made with the new PBI block copolymers. The long-term ability to sustain higher loads was also remarkably improved as demonstrated by a continuous $>$ 2000 h test at 0.2 A/cm^2 with low degradation rate. The overall performance was comparable to meta-PBI, but with significant modifications of the acid and polymer loadings, membrane mechanical behavior, and swelling behavior. The electrode pretreatment approach should allow a more thorough evaluation of PBI block copolymer compositions and further tuning of full suite of membrane properties needed for successful fuel cell operations.

ACKNOWLEDGMENTS

The first author would like to thank BASF, and in particular Dr. von Bernstorff and Dr. Grösser for providing a fellowship for a postdoctoral stay with Prof. Benicewicz at the University of South Carolina (USA). Furthermore, the authors thank Dr. Calundann from former BASF Fuel Cell (New Jersey) for financial support and his interest in this work. The authors would like to dedicate this paper to the memory of Prof. James McGrath, a pioneer in the field of polymer membranes and close friend.

REFERENCES AND NOTES

1 J. M. Larson, S. J. Hamrock, G. M. Haugen, P. Pham, W. M. Lamanna, A. B. Butenhoff Moss, *J. Power Sources* **2007**, *172*, 108–114.

2 Q. Li, J. O. Jensen, R. F. Savinell, N. J. Bjerrum, *Prog. Polym. Sci.* **2009**, *34*, 449–477.

3 A. Chandan, M. Hattenberger, A. El-kharouf, S. Du, A. Dhir, V. Self, B. G. Pollet, A. Ingram, W. Bujalski, *J. Power Sources* **2013**, *231*, 264–278.

4 A. Carollo, E. Quartarone, C. Tomasi, P. Mustarelli, F. Belotti, A. Magistris, F. Maestroni, M. Parachini, L. Garlaschelli, P. P. Righetti, *J. Power Sources* **2006**, *160*, 175–180.

5 J. Mader, L. Xiao, T. J. Schmidt, B. C. Benicewicz, *Adv. Polym. Sci.* **2008**, *216*, 63–124.

6 J. A. Asensio, S. Borrós, P. Goméz-Romero, *J. Electrochem. Soc.* **2004**, *151*, A304–A310.

7 G. Qian, D. W. Smith, B. C. Benicewicz, *Polymer* **2009**, *50*, 3911–3916.

8 J. Yang, Y. Xu, L. Zhou, Q. Che, R. He, Q. Li, *J. Memb. Sci.* **2013**, *446*, 318–325.

9 D. Aili, M. K. Hansen, C. Pan, Q. Li, E. Christensen, J. O. Jensen, N. J. Bjerrum, *Int. J. Hydrogen Energy* **2011**, *36*, 6985–6993.

10 P. Mustarelli, E. Quartarone, S. Grandi, S. Angioni, A. Magistris, *Solid State Ionics* **2012**, *225*, 228–231.

11 P. Noyé, Q. Li, C. Pan, N. J. Bjerrum, *Polym. Adv. Technol.* **2008**, *19*, 1270–1275.

12 S. Wang, G. Zhang, M. Han, H. Li, Y. Zang, J. Ni, W. Ma, M. Li, J. Wang, Z. Liu, L. Zhang, H. Na, *Int. J Hydrogen Energy* **2011**, *36*, 8412–8421.

13 M. Li, G. Zhang, H. Zuo, M. Han, C. Zhao, H. Jiang, Z. Liu, L. Zhang, H. Na, *J. Memb. Sci.* **2012**, *423–424*, 495–502.

14 J. Su, H. Pu, Z. Chang, D. Wan, *Polymer* **2012**, *53*, 3587–3593.

15 H. L. Liu, Y. C. Chou, T. L. Yu, S. W. Lai, *Int. J. Hydrogen Energy* **2012**, *37*, 383–392.

16 P. Staiti, M. Minutoli, *J. Power Sources* **2001**, *94*, 9–13.

17 T. Ossiander, C. Heinzl, S. Gleich, F. Schönberger, P. Völk, M. Welsch, C. Scheu, *J. Memb. Sci.* **2014**, *454*, 12–19.

18 F. Schönberger, J. Kerres, *J. Polym. Sci. Part A: Polym. Chem.* **2007**, *45*, 5237–5255.

19 A. Taeger, C. Volen, D. Lehmann, W. Lenk, K. Schlenstedt, J. Meier-Haack, *J. Macromol. Symp.* **2004**, *210*, 175–184.

20 A. Roy, M. A. Hickner, X. Yu, Y. Li, T. E. Glass, J. E. McGrath, *J. Polym. Sci. Part B: Polym. Phys.* **2006**, *44*, 2226–2239.

21 H. S. Lee, A. Roy, O. Lane, J. E. McGrath, *Polymer* **2008**, *49*, 5387–5396.

22 F. Schönberger, A. Chromik, J. Kerres, *Polymer* **2010**, *51*, 4299–4313.

23 C. Zhao, H. Lin, M. Han, H. Na, *J. Memb. Sci.* **2010**, *353*, 10–16.

24 S. B. Darling, *Prog. Polym. Sci.* **2007**, *32*, 1152–1204.

25 M. S. Yung, T. H. Kim, Y. J. Yoon, C. G. Kang, J. Y. Lee, H. J. Kim, Y. T. Hong, *J. Memb. Sci.* **2014**, *459*, 72–85.

26 H. Ghassemi, J. E. McGrath, T. A. Zawodzinski, *Polymer* **2006**, *47*, 4132–4139.

27 D. M. Knauss, J. E. McGrath, T. Kashiwagi, In 208th National Meeting, ACS Symposium Series 599, August 21–26, 1994; American Chemical Society: Washington, DC, **1995**; pp 41–55.

28 M. J. Jurek, J. E. McGrath, *Polymer* **1989**, *30*, 1552–1557.

29 M. J. Kunz, G. Hayn, R. Saf, W. H. Binder, *J. Polym. Sci. Part B: Polym. Chem.* **2004**, *42*, 661–674.

30 G. Hardie, *J. Histochem. Cytochem.* **1982**, *30*, 1082–1085.

31 K. I. Hirai, *J. Histochem. Cytochem.* **1971**, *19*, 434–442.

32 L. Xiao, H. Zhang, E. Scanlon, L. S. Ramanathan, E. W. Choe, D. Rogers, T. Apple, B. C. Benicewicz, *Chem. Mater.* **2005**, *17*, 5328–5333.

33 G. Odian, Principles of Polymerization; Wiley: New Jersey, **2004**; pp 29–32.

34 T. G. Fox, P. J. Flory, *J. Appl. Phys.* **1950**, *21*, 581–591.

35 H. Pu, W. H. Meyer, G. Wegner, *J. Polym. Sci. Part B: Polym. Phys.* **2002**, *40*, 663–669.

36 Z. Liu, J. S. Wainright, R. F. Savinell, *Chem. Eng. Sci.* **2004**, *59*, 4833–4838.

37 R. Bouchert, S. Miller, M. Duclot, J. L. Souquet, *Solid State Ionics* **2001**, *145*, 69–78.

38 R. Bouchert, E. Siebert, *Solid State Ionics* **1999**, *118*, 287–299.

39 P. A. Staniland, C. J. Wilde, *Polymer* **1992**, *33*, 1976–1981.

40 D. J. Riley, A. Gungor, S. A. Srinivasan, M. Sankarapandian, C. Tchatchoua, M. W. Muggli, T. C. Wand, J. E. McGrath, *Polym. Eng. Sci.* **1997**, *37*, 1501–1511.

41 H.-G. Elias, Makromoleküle: Physikalische Strukturen und Eigenschaften; Wiley-VCH: Weinheim; Kapitel, **2001**, Vol. *13*, pp 452–469.

42 M. Eikerling, A. A. Kornyshev, A. M. Kuznetsov, J. Ulstrup, S. Walbran, *J. Phys. Chem. B* **2001**, *105*, 3646–3662.

43 S. Galbiati, A. Baricci, A. Casalegno, R. Marchesi, *Int. J. Hydrogen Energy* **2013**, *38*, 6469–6480.

44 M. A. Molleo, X. Chen, H. J. Ploehn, K. J. Fishel, B. C. Benicewicz, *Fuel Cells* **2014**, *14*, 16–25.